Nano Research

Open Access

Research Article

Enhanced oral drug delivery by mimicking natural amino acid and oligopeptide absorption route

Ruinan Wu[1,§], Xiaoxing Fan[1,§], Licheng Wu[1], Liyun Xing[1], Jinxia Kong[1], Zhou Zhou[1], Jingyuan Wen[2], Lian Li[1]✉, and Yuan Huang[1]✉

[1] *Key Laboratory of Drug-Targeting and Drug Delivery System of the Education Ministry and Sichuan Province, Sichuan Engineering Laboratory for Plant-Sourced Drug and Sichuan Research Center for Drug Precision Industrial Technology, West China School of Pharmacy, Sichuan University, Chengdu 610041, China*

[2] *School of Pharmacy, Faculty of Medical and Health Sciences, University of Auckland, Auckland 1023, New Zealand*

[§] *Ruinan Wu and Xiaoxing Fan contributed equally to this work.*

Cite this article: *Nano Research*, **2025**, *18*, 94907082. https://doi.org/10.26599/NR.2025.94907082

ABSTRACT: Oral delivery of protein and peptide drugs presents considerable challenges due to their susceptibility to digestive enzymes in gastrointestinal (GI) tract and low efficiency of transepithelial transport. Herein, inspired by efficient absorption of protein-based nutrients, we constructed several kinds of oral drug delivery systems by mimicking natural amino acid and oligopeptide absorption route. Three kinds of amino acids and two kinds of oligopeptides were chosen as targeting ligands to mediate transportation of orally administered nanoparticles (NPs). Liraglutide (Lira), a kind of glucagon like peptide-1 (GLP-1) receptor agonist, was used as model drug. These functionalized NPs could protect Lira from enzymatic degradation in GI tract. Moreover, compared with amino acid-modified NPs, oligopeptide-modified NPs exhibited greater transepithelial transport efficiency and were primarily absorbed in the proximal small intestine due to the high expression and transportation mediated by proton coupled oligopeptide transporter 1 (PEPT1). These Lira-loaded NPs could effectively control the blood glucose level, reduce plasma lipid level, and repair tissue damage on type 2 diabetic mice and even showed comparable hypoglycemic effects of subcutaneous injection (s.c.) free Lira. Our study demonstrates the potential of mimicking natural oligopeptide absorption route to enhance oral delivery of protein and peptide drugs.

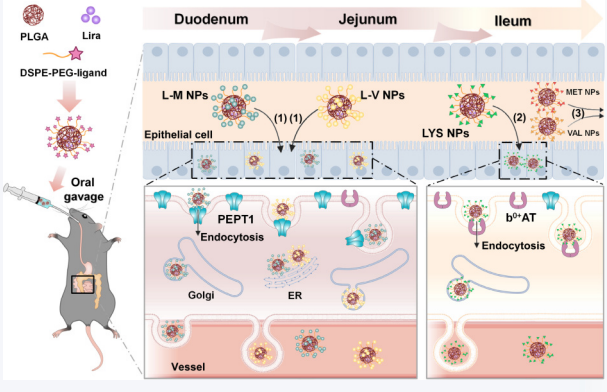

KEYWORDS: oral drug delivery, amino acid absorption route, oligopeptide absorption route, liraglutide

1 Introduction

Protein and peptide drugs are mainly administered by injection, but the repetitive injection results in needle phobia and various injection-related side effects [1–3]. Oral administration is a simple and more acceptable administration route, which can overcome some problems caused by injection and is beneficial for the treatment of chronic diseases requiring long-term medication [4–6]. However, the degradation of protein and peptide drugs in harsh environment of gastrointestinal tract and the permeation of these biomacromolecular drugs through epithelium remain a challenge and thereby limit their clinical application [7, 8].

Commonly, as basic nutrients, some amino acids and oligopeptides are efficiently absorbed by the small intestine [9–11]. It has been reported that up to 100 g of amino acids and oligopeptides are absorbed by the small intestine every day to maintain the normal physiological functions of the human body [12, 13]. Such efficient absorption can be attributed to multiple transport systems presented in the intestinal epithelium, such as amino acid transporters and proton coupled oligopeptide transporter 1 (PEPT1) [14–16]. Therefore, inspired by the efficient absorption of amino acids and oligopeptides in the small intestine, it is potential to turn this challenge into an opportunity to construct an oral delivery system by mimicking the absorption route of natural amino acids and oligopeptides.

Received: July 29, 2024; **Revised:** September 23, 2024
Accepted: October 17, 2024

✉Address correspondence to Yuan Huang, huangyuan0@163.com; Lian Li, liliantripple@163.com

However, different kinds of amino acids (cationic amino acids, neutral amino acids, and anionic amino acids) and oligopeptides exhibit varying absorption characteristics. Of note, it is reported that only cationic and neutral amino acids can be transported unidirectionally from the apical side to the basolateral side of epithelial cells and then enter into blood circulation [17–19]. Hence, in order to construct efficient oral delivery systems simulating the natural transport routes, we also need to explore: (1) Does this constructed drug delivery system facilitate the oral delivery of protein and peptide drugs and the treatment of related chronic diseases? (2) Which of the simulated amino acid and oligopeptide transport strategies is more suitable for oral drug delivery?

Herein, three kinds of amino acids (lysine (LYS), methionine (MET), and valine (VAL)) and two kinds of oligopeptides (lysine-methionine (L-M) and lysine-valine (L-V)) were used as targeting ligands to mediate transportation of orally administered nanoparticles (NPs). Liraglutide (Lira), a glucagon like peptide-1 (GLP-1) receptor agonist, was chosen as model drug. Firstly, the pharmacokinetic behavior and hypoglycemic activity of above mentioned NPs were investigated. Subsequently, the underlying mechanisms were further revealed by *in vitro* cell experiments and the intestinal tissue models. Finally, the long-term pharmacodynamics and safety were evaluated. The results showed that, compared to the amino acid ligand, oligopeptide-modified NPs could improve the oral bioavailability of Lira more efficiently. They had higher transepithelial transport efficiency and were primarily absorbed in the proximal small intestine due to the high expression and transportation mediated by PEPT1. On type 2 diabetic mice, these oligopeptide-modified Lira-loaded NPs could effectively control the blood glucose level, reduce plasma lipid level, and repair tissue damage, and even showed comparable hypoglycemic effects of subcutaneous injection (s.c.) free Lira. Our study demonstrates that the natural oligopeptide absorption-mimicking oral drug delivery systems show promising application potential in the treatment of chronic diseases.

2 Materials and methods

2.1 Materials

Poly(lactic-co-glycolic acid) (PLGA) with one methoxy end group was purchased from Lactel absorbable polymers (California, USA). 1,2-Distearoyl-sn-glycero-3-phosphoethanolamine-N-[methoxy(polyethyleneglycol)] (DSPE-PEG) and an amino end group (DSPE-PEG-NH_2) were obtained from Ponsure Biological Co., Ltd. (Shanghai, China). N,N'-Di-boc-l-lysine hydroxy succinimide ester (Boc-Lys(Boc)-OSu), tert-butoxycarbonyl-l-valine n-hydroxysuccinimide ester (Boc-Val-OSu), 2,5-dioxo-1-pyrrolidinyl n-(((2-methyl-2-propanyl)oxy)carbonyl) methioninate (Boc-Met-OSu), and (S)-2,5-dioxopyrrolidin-1-yl-6-(((benzyloxy) carbonyl)amino)-2-((tert-butoxycarbonyl)amino)hex-anoate (Boc-Lys(Z)-OSu) were purchased from Aladdin Reagent Co., Ltd. (Shanghai, China). Soybean phospholipid was purchased from Shanghai Tywei Pharmaceutical Co., Ltd. (China). Lira was provided by HEC Pharmaceutical (Guangdong, China). All other reagents were purchased from commercial products of analytical or reagent grade.

2.2 Synthesis of DSPE-PEG-LYS/MET/VAL

DSPE-PEG-LYS/MET/VAL was synthesized by conjugating DSPE-PEG-NH_2 with the carboxyl groups of amino acids. Briefly, DSPE-PEG-NH_2 (56 mg) and Boc-Lys(Boc)-OSu (26.6 mg)/Boc-Met-OSu (20.8 mg)/Boc-Val-OSu (18.9 mg) were dissolved in dichloromethane (2 mL). Triethylamine (50 μL) was added dropwise to the system and the mixture was stirred at 30 °C for 24 h. Subsequently, trifluoroacetic acid (1 mL) was added to the mixture and the reaction was maintained for 6 h under stirring. Finally, dichloromethane and trifluoroacetic acid were removed by rotary evaporation. The resultant mixture was dialyzed against deionized water for 48 h and the products were obtained after lyophilization.

2.3 Synthesis of DSPE-PEG-L-M and DSPE-PEG-L-V

At first, DSPE-PEG-Lys(Z) was synthesized by conjugating Boc-Lys(Z)-OSu to DSPE-PEG-NH_2 via an amido bond. Briefly, DSPE-PEG-NH_2 (56 mg) and Boc-Lys(Z)-OSu (28.7 mg) were dissolved in dichloromethane (2 mL). Triethylamine (50 μL) was added dropwise to the system and the mixture was stirred at 30 °C for 24 h. Trifluoroacetic acid (1 mL) was added to the mixture and the reaction was maintained for 6 h under stirring. After dichloromethane and trifluoroacetic acid were removed by rotary evaporation, the resultant mixture was dialyzed against deionized water for 48 h. DSPE-PEG-Lys(Z) was obtained after lyophilization. Subsequently, DSPE-PEG-Lys(Z) (60 mg) and Boc-Met-OSu (20.8 mg)/Boc-Val-OSu (18.9 mg) were dissolved in dichloromethane (2 mL) and then triethylamine (50 μL) was added. The mixture was stirred at 30 °C for 24 h. Trifluoroacetic acid (1 mL) was added and kept stirring for 6 h. Dichloromethane and trifluoroacetic acid were removed by rotary evaporation. The residue obtained was dissolved in ethyl acetate (2 mL), following the addition of palladium carbon (8 mg). The reaction was continued for 6 h under stirring at 1000 rpm in hydrogen. The resultant mixture was then centrifuged at 10,000 rpm for 10 min and the supernatant was collected, followed by rotary evaporation to remove the solvent. The mixture was dialyzed against deionized water for 48 h and the products were obtained after lyophilization. The functionalized polymers were verified by nuclear magnetic resonance (NMR) spectroscopy and Fourier transform infrared (FTIR) spectroscopy. Meanwhile, the proportion of functionalized DSPE-PEG was analyzed by ninhydrin reaction.

2.4 Preparation and characterization of NPs

Unmodified PLGA NPs (PEG NPs) and a variety of protein-based nutrients-modified PLGA NPs were prepared by self-assembly nanoprecipitation method [20]. Protein-based nutrients-modified NPs include lysine-modified NPs (LYS NPs), methionine-modified NPs (MET NPs), valine-modified NPs (VAL NPs), lysine-methionine-modified NPs (L-M NPs), and lysine-valine-modified NPs (L-V NPs). In details, PLGA, functionalized DSPE-PEG, soybean lecithin, and Lira were dissolved in dimethyl sulfoxide (DMSO) at a mass ratio of 5:2:2:1. Subsequently, the mixture solution was slowly dropped into the deionized water (1 mL) under stirring at 1000 rpm for 10 min. DMSO, free polymers, and free drug were removed by ultrafiltration (6000 rpm, 10 min) with a molecular weight cut-off (MWCO) of 100 kDa. At last, the NPs were redispersed in deionized water or other mediums for the follow-up experiments. For the preparation of fluorescence-labeled NPs, fluorescein isothiocyanate (FITC)-Lira was added in the formulation to replace Lira and the other procedures were identical.

For NPs characterization, dynamic light scattering (DLS) diameter and zeta potential were measured by Zetasizer Nano ZS90

(Malvern Instruments Ltd., UK). The morphology of NPs was observed by transmission electron microscopy (TEM). The encapsulation efficiency (EE) and drug loading (DL) of Lira-loaded NPs were determined via ultrafiltration. Briefly, the freshly prepared Lira-loaded NPs were placed in centrifuge tubes (MWCO of 100 kDa) and the free Lira was isolated by ultrafiltration (6000 rpm, 10 min). The content of loaded and free Lira was measured by high-performance liquid chromatography (HPLC, Agilent 1260 series) on a Diamonsil C18 column (150 mm × 4.6 mm, 5 μm). Trifluoroacetic acid aqueous solution (0.2%) and acetonitrile at a ratio of 50:50 (v/v) was used as the mobile phase. Detection wavelength was set at 214 nm and the flow rate of eluent was 1 mL/min. All assays were conducted in triplicate. The EE and DL were calculated using Eqs. (1) and (2)

$$\text{EE}\ (\%) = \frac{\text{Lira loaded in nanoparticles}}{\text{Lira loaded in nanoparticles} + \text{free Lira}} \times 100\% \quad (1)$$

$$\text{DL}\ (\%) = \frac{\text{Lira loaded in nanoparticles}}{\text{weight of nanoparticles}} \times 100\% \quad (2)$$

The colloidal stability of Lira-loaded NPs in simulated gastral fluid (SGF) and simulated gastral fluid (SIF) was studied by measuring the particle size within 12 h at 37 °C. The release profile of Lira-loaded NPs was studied. In brief, Lira-loaded NPs were placed into a dialysis tube (MWCO of 100 kDa) and then immersed in SGF or SIF at 37 °C. At determined time points, 100 μL of Lira-loaded NPs was taken out and DMSO was added to destroy the NPs. The remained Lira of NPs was measured quantitatively by HPLC. To investigate the protection of NPs for Lira against trypsin, Lira-loaded NPs were dispersed in SIF containing trypsin and incubated for 4 h at 37 °C. At determined time points, 100 μL of Lira-loaded NPs was withdrawn and mixed with DMSO containing 2% trifluoroacetic acid. The remained Lira of NPs was measured quantitatively by HPLC.

2.5 *In vivo* pharmacokinetic and pharmacodynamic studies

All animal study protocols were approved by the Institutional Animal Care and Use Committee at Sichuan University. For pharmacokinetic study, ICR mice were fasted overnight with free access to water. Then, the mice were administered with CY5-Lira-loaded NPs (CY5-Lira NPs, 5 mg/kg of CY5-Lira) by oral gavage. s.c. of CY5-Lira solution (0.5 mg/kg) and oral administration of CY5-Lira solution (5 mg/kg) were used as controls. At predetermined time points, blood samples were collected from the orbit. The concentration of Cy5-Lira was quantified by Fluorescence Microplate Reader. Area under the curve (AUC) of plasma Cy5-Lira concentration versus time was calculated. The relative bioavailability (Fr%) to subcutaneous injection was calculated with Eq. (3)

$$\text{Fr}\% = \frac{\text{AUC (oral)} \times \text{dose (SC)}}{\text{AUC (SC)} \times \text{dose (oral)}} \times 100\% \quad (3)$$

The intraperitoneal injection glucose tolerance test (IPGTT) was conducted to evaluate the hypoglycemic activity of different formulations. Type 2 diabetes db/db mice were fasted for 5 h and then administered by oral gavage with Lira-loaded NPs (Lira NPs, 5 mg/kg of Lira) and Lira solution (5 mg/kg), or by subcutaneous injection with Lira solution (0.5 mg/kg). 1 h later, glucose solution (2 g/kg) was injected intraperitoneally. At predetermined time points, blood samples were collected from the tail vein and the blood glucose levels were measured with a glucose meter.

2.6 Mucus permeation study

In brief, 50 μL of fresh porcine intestinal mucus was added into the apical chamber and 800 μL of PBS was added into the basolateral chamber. Next, 200 μL of FITC-Lira-loaded NPs (FITC-Lira NPs) was carefully placed onto the mucus layer and the system was incubated at 37 °C. At the predetermined time points, samples (80 μL) were withdrawn from the basolateral chamber and blank phosphate buffered saline (PBS, 80 μL) was added. The fluorescence intensity was measured by Varioskan Flash multimode reader. The apparent permeability coefficient (Papp) was calculated using Eq. (4)

$$\text{Papp} = \frac{\text{d}Q}{\text{d}T} \times \frac{1}{A \times C_0} \quad (4)$$

where dQ/dT is the flux of FITC-Lira from the apical chamber to the basolateral chamber, C_0 is the initial concentration of FITC-Lira loaded in NPs in the apical chamber, and A is the membrane area (cm^2).

2.7 Cellular uptake study

Caco-2 cells were seeded in 96-well plates at the density of 1 × 10^4 cells/well and cultured for 3 days. FITC-Lira NPs were co-incubated with cells at 37 °C for 2 or 4 h. Afterward, the above mentioned NPs were removed and the cells were washed by PBS for three times. DMSO was added and the intracellular fluorescence intensity (485/520 nm) was measured by the Varioskan Flash multimode reader.

To investigate the endocytic mechanisms of amino acid and oligopeptide-modified NPs, the substrates or regulators of the related transporters were used. Caco-2 cells were seeded in 96-well plates at the density of 1 × 10^4 cells/well and cultured for 3 days. LYS (20 mM), MET (20 mM), VAL (20 mM), glycine (GLY, 50 mM), glycylsarcosine (Glysar, 50 mM), and insulin (5 nM) were respectively preincubated with Caco-2 cells at 37 °C for 30 min. Afterward, the cells were incubated with FITC-Lira NPs for 4 h. The cells were washed by PBS for three times followed by the addition of DMSO. The internalization was analyzed by the Varioskan Flash multimode reader.

The expression of blastocyst neutral and cationic amino acid transporter ($b^{0,+}$AT), broad neutral amino acid transporter 1 (B^0AT1), and PEPT1 on Caco-2 cells was characterized by immunofluorescence staining. Caco-2 cells were seeded on Transwell inserts at the density of 5 × 10^4 cells/well and cultured for 14–21 days until the transepithelial electrical resistant (TEER) values were up to 300 Ω·cm^2. NPs were incubated with cell monolayers at 37 °C for 12 h. And then cells were fixed with 4% paraformaldehyde for 15 min and incubated with 0.2% Triton X-100 for 5 min. After incubated with 5% goat serum for 30 min, cell monolayers were incubated with specific primary antibodies overnight at 4 °C and goat anti-rabbit IgG Alexa Fluor594 for 1 h at 37 °C. Afterwards, the nucleus was stained with Hoechst 33342 for 5 min and the expression of transporters was observed with confocal laser scanning microscopy (CLSM).

2.8 Transcytosis study

Caco-2 cells were seeded on Transwell inserts at the density of 5 × 10^4 cells/well and cultured for 14–21 days until the TEER values were up to 300 Ω·cm^2. FITC-Lira NPs were added to the apical chamber and blank HBSS was added to the basolateral chamber. At

determined time points, samples (80 μL) were withdrawn from the basolateral chamber and blank Hanks' balanced salt solution (HBSS, 80 μL) was added. The fluorescence intensity was measured by Varioskan Flash multimode reader. The Papp was calculated using Eq. (5)

$$\text{Papp} = \frac{dQ}{dT} \times \frac{1}{A \times C_0} \quad (5)$$

where dQ/dT is the flux of FITC-Lira from the apical chamber to the basolateral chamber, C_0 is the initial concentration of FITC-Lira loaded in NPs in the apical chamber, and A is the membrane area (cm^2).

2.9 Intracellular trafficking study

For the quantitative study, Caco-2 cells were seeded in 96-well plates at the density of 1×10^4 cells/well and cultured for 3 days. FITC-Lira NPs were pre-incubated with cells at 37 °C for 2 h. Then the cells were treated with blank HBSS, LY294002 (1 mM), brefeldin A (25 μg/mL), and monensin (33 μg/mL) for 2 h, respectively [21]. The intracellular fluorescence intensity was measured by the Varioskan Flash multimode reader. The colocalization of FITC-Lira NPs with different subcellular organelles was analyzed by CLSM. In brief, Caco-2 cells were seeded on sterile coverslips at the density of 1×10^5 cells/well and cultured for 3–4 days. After incubation with FITC-Lira NPs at 37 °C for 1 h, the cells were divided into three groups and treated as follows: One group was treated with ER-tracker Red at 37 °C for 0.5 h; another group was treated with GA-tracker Red at 4 °C for 0.5 h, followed by incubation with fresh DMEM at 37 °C for 0.5 h; and the last group was treated with lysosome-tracker Red at 37 °C for 1 h. Then, the cells were fixed by 4% paraformaldehyde for 15 min. Hoechst 33342 was used to stain the nucleus before CLSM observation. Pearson's correlation coefficient (Pr) was calculated by Image-Pro Plus.

2.10 Intestinal absorption of NPs

An *in situ* intestinal loop model was used to evaluate the intestinal absorption of NPs [22]. Sprague Dawley (SD) rats were fasted for 24 h with free access to water. The abdominal cavity was opened under anaesthetic. FITC-Lira NPs were injected into the intestinal loops (2 cm) which were ligated at both ends. After 2 h, rats were euthanized and the intestinal loops were collected. The intestinal lumens were gently rinsed with PBS and fixed with 4% paraformaldehyde overnight. After dehydrated with 30% sucrose, the intestinal lumens were embedded with optimal cutting temperature (OCT) compound followed by frozen section (10 μm). Hoechst 33342 was used to stained the nucleus. The sections were visualized with CLSM.

To observe the expression of b^{0+}AT and PEPT1 in different sections of the small intestine, duodenum, jejunum, and ileum were collected from SD rats and treated as the procedures above mentioned. After frozen section (10 μm), the sections were incubated with 5% goat serum for 1 h at 37 °C. The immune-fluorescent staining of b^{0+}AT and PEPT1 was conducted by incubating with specific primary antibodies overnight at 4 °C and goat anti-rabbit IgG Alexa Fluor594 for 2 h. The nucleus was stained with Hoechst 33342 and the sections were visualized with CLSM.

Ex vivo intestinal permeation was conducted to further quantitatively study the permeation profiles of NPs. 2 cm of duodenum, jejunum, and ileum were cut off from sacrificed rats and FITC-Lira NPs were injected to the ligated intestinal loops. Subsequently, the intestinal loops were immersed in Krebs–Ringer (K–R) solution and incubated at 37 °C accompanied with shaking. At the determined time point, 80 μL solution was withdrawn followed by the supplement of 80 μL K–R solution. The amount of FITC-Lira in the samples was measured by Varioskan Flash multimode reader. The Papp was calculated using Eq. (6)

$$\text{Papp} = \frac{dQ}{dT} \times \frac{1}{A \times C_0} \quad (6)$$

where dQ/dT is the flux of FITC-Lira from the ligated intestinal loops to the K–R solution, C_0 is the initial concentration of FITC-Lira in the ligated intestinal loops, and A is the surface area of ligated intestinal loops (cm^2).

2.11 Long-term pharmacodynamic study

For the long-term therapeutic evaluation, the db/db mice were orally administrated with free Lira (denoted as oral free Lira), Lira PEG NPs, Lira LYS NPs, Lira L-M NPs, and Lira L-V NPs, respectively, and subcutaneously injected with Lira (denoted as s.c. free Lira) once a day for 28 days. The fasting blood glucose (FBG) of mice was recorded at the predetermined time points. After 28 days, the db/db mice were sacrificed and the content of glycated hemoglobin (HbA1c), insulin, and hepatic glycogen in plasma was measured, respectively. In addition, the content of creatinine, Urea, cholesterol (CHO), triglyceride (TG), high-density lipoprotein cholesterol (HDL-C), and low-density lipoprotein cholesterol (LDL-C) was evaluated by blood biochemical instrument (COBAS C311, Roche Diagnostics GMBH). Pancreas was fixed by 4% paraformaldehyde, dehydrated by ethanol, and embedded by paraffin. Then, the pancreas was sliced for immunohistochemical staining of insulin and glucagon in the islets. Briefly, the sections of pancreas were incubated with mouse anti-insulin primary antibody or rabbit anti-glucagon primary antibody, respectively, at 37 °C for 1 h, and then incubated with goat anti-mouse IgG Alexa Fluor 488 or donkey anti-rabbit IgG Alexa Fluor647, respectively, at 37 °C for 45 min. The nucleus was stained with Hoechst 33342 and the sections were visualized with CLSM. The morphology of pancreas was also assessed by hematoxylin and eosin (H&E) staining. Liver and epididymal visceral adipose tissue were also collected and assessed by Oil red O staining.

2.12 *In vivo* safety evaluation of NPs

Healthy ICR mice were orally given saline solution, PEG NPs, L-M NPs, and L-V NPs once a day for 28 days, respectively. After 28 days, the mice were sacrificed and the blood samples were collected for blood routine and biochemical tests. In addition, the major organs including heart, liver, spleen, lung, kidney, and the small intestine were collected and fixed by 4% paraformaldehyde for H&E staining.

2.13 Statistical analyses

The data were presented as mean ± standard deviation (SD). Difference between two groups was analyzed by two tail Student's *t*-test. When comparing multiple groups, one-way analysis of variance (ANOVA) was performed. $p < 0.05$ was considered significant.

3 Results and discussion

3.1 Synthesis of functionalized polymers

Amino acid or oligopeptide modified DSPE-PEG was obtained by

conjugating DSPE-PEG-NH_2 with specific ligands by covalent amide reactions (Fig. 1(a)). The structure of the functionalized DSPE-PEG was verified by proton ^{1}H-NMR spectroscopy (Figs. S1 and S2 in the Electronic Supplementary Material (ESM)). The characteristic peaks of DSPE-PEG-LYS were similar to the chemical shifts of DSPE-PEG-NH_2, but the peak at 1.37 ppm, corresponding to the residual Boc protecting group of LYS, indirectly confirmed the successful binding of LYS to DSPE-PEG-NH_2. The structure of

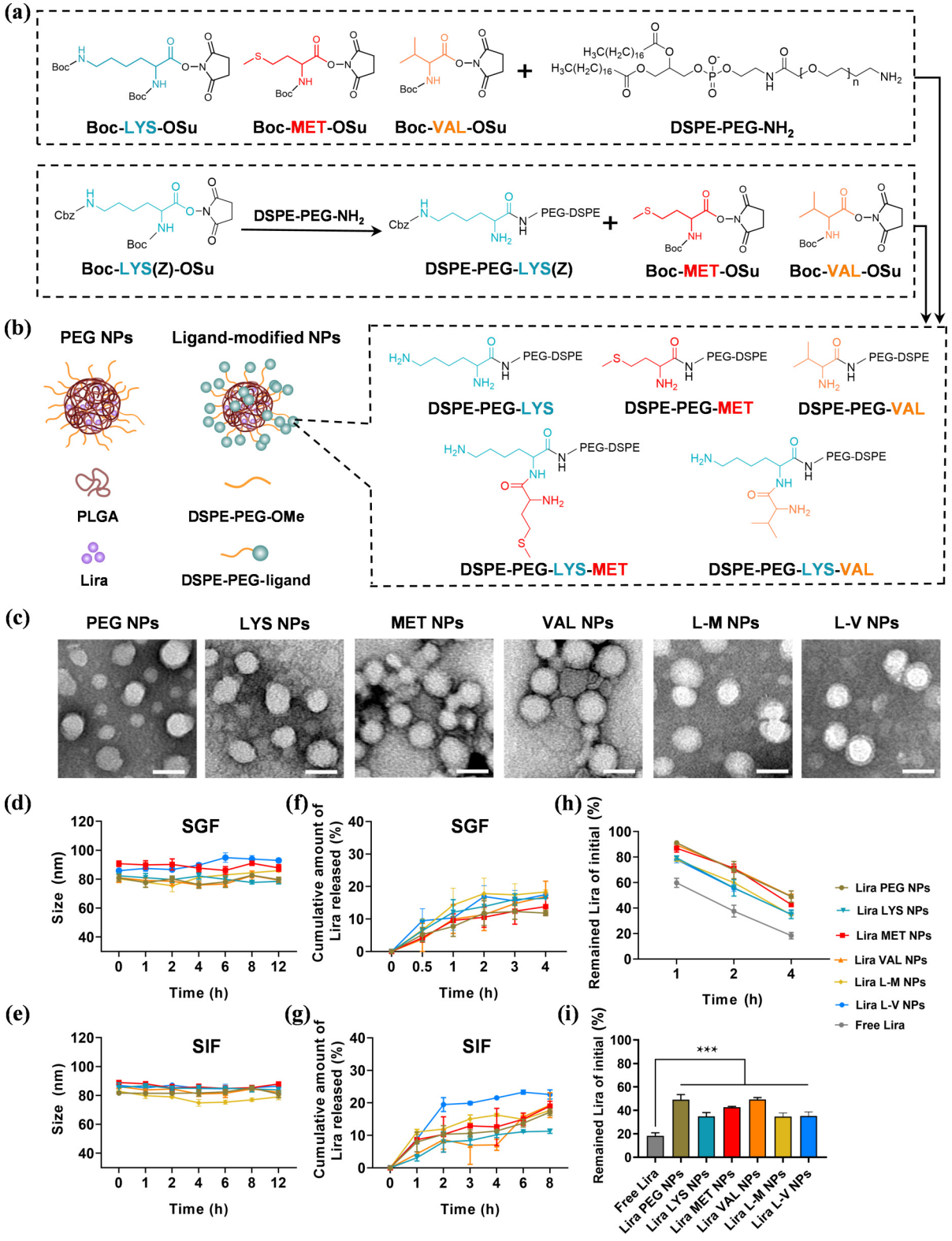

Figure 1 Preparation and characterization of nanoparticles. (a) Synthetic procedures of functionalized polymers. (b) Illustration of nanoparticles. (c) TEM images. Scale bar = 50 μm. (d) and (e) Stability of nanoparticles in SGF and SIF. (f) and (g) Release profiles of Lira loaded in nanoparticles in SGF and SIF. (h) Trypsin degradation evaluation of Lira in different nanoparticles. (i) Remained percentage of Lira after incubation with trypsin for 4 h. ***$p < 0.001$. Mean ± SD ($n = 3$).

DSPE-PEG-MET was confirmed by the characteristic peak at 2.05 ppm, attributed to the methyl group of MET, while the structure of DSPE-PEG-VAL was confirmed by the peak at 0.92 ppm, assigned to the methyl group of VAL. The characteristic peaks around 7.48–7.13 ppm, corresponding to the benzene ring structure of Cbz protecting group, appeared in the spectrum of DSPE-PEG-LYS(Z). The disappearance of Cbz protecting group peaks, accompanied by the emergence of peaks at 2.05 ppm in the DSPE-PEG-L-M spectrum and 0.92 ppm in the DSPE-PEG-L-V spectrum, indicated the successful conjugation of oligopeptides. FTIR spectroscopy was further performed to identify the functional groups (Fig. S3 in the ESM). The FTIR spectra of DSPE-PEG-NH_2 revealed characteristic peaks at 3300–3500 cm^{-1} corresponding to amidogen (N–H). The disappearance or transformation of the amidogen (N–H) absorption band confirmed that the ligands had conjugated with the DSPE-PEG-NH_2 indirectly.

Meanwhile, the ligand modification efficiency of functionalized polymers was measured by ninhydrin reaction. The percentage of ligand modification of DSPE-PEG-LYS, DSPE-PEG-MET, DSPE-PEG-VAL, DSPE-PEG-L-M, and DSPE-PEG-L-V was 81 mol%, 79 mol%, 84 mol%, 61 mol%, and 63 mol%, respectively.

3.2 Preparation and characterization of NPs

NPs were fabricated via nanoprecipitation method. Lira and PLGA constituted the core of NPs while DSPE-PEG-ligand was inserted on the surface (Fig. 1(b)). All the NPs exhibited good monodispersity with the diameter of 80–90 nm (Table S1 in the ESM). The morphology of NPs was characterized by TEM and the results showed a spherical shape for all the NPs (Fig. 1(c)). The zeta potential of ligand-modified NPs increased compared to PEG NPs due to the protonation of free –NH_2 groups being presented in the amino acid and oligopeptide. The EE and DL were about 90% and 15%, respectively (Table S1 in the ESM).

To evaluate the stability of NPs, the particle size was monitored in SGF or SIF by DLS for 12 h (Figs. 1(d) and 1(e)). All the NPs exhibited almost unchanged particle size within 12 h, implying their good stability. A slow release profile of Lira was observed and the cumulative release amount was approximately 20% in SGF within 4 h (Fig. 1(f)) and also approximately 20% in SIF within 8 h (Fig. 1(g)). Of note, no burst release phenomenon was observed either in SGF or in SIF. It was demonstrated that Lira could be well encapsulated in PLGA NPs. Furthermore, all the NPs could protect Lira from trypsin degradation (Figs. 1(h) and 1(i)) with remained amount of 34.7%–49.3% which was significantly higher compared to free Lira (18.3%) after incubation with trypsin for 4 h. This might be attributed to the dense polymer network of PLGA NPs, which could prevent the direct contact between Lira and trypsin, thereby protecting Lira from degradation.

3.3 Oligopeptide-modified NPs exhibited more efficient drug delivery *in vivo* compared to the amino acid-modified NPs

To evaluate the drug delivery efficiency of NPs *in vivo*, the pharmacokinetic experiment was conducted (Figs. 2(a) and 2(b)). ICR mice were administrated with different formulations and the plasma concentration of Cy5-Lira at each time point was measured. PEG NPs and neutral amino acid-modified NPs (MET/VAL NPs) showed 4.3%–5.5% of Fr, which had no significant difference with free Cy5-Lira ($p > 0.05$), except cationic amino acid-modified NPs (LYS NPs) exhibiting enhanced absorption with Fr of 6.2% ($p < 0.05$). The results indicated that the type of amnio acid ligand might have an influence on the drug delivery efficiency of ligand-modified NPs. It should be noted that oligopeptide-modified NPs (L-M/L-V NPs) showed a higher peak concentration (C_{max}) and AUC compared to amino acid-modified NPs. L-M NPs and L-V

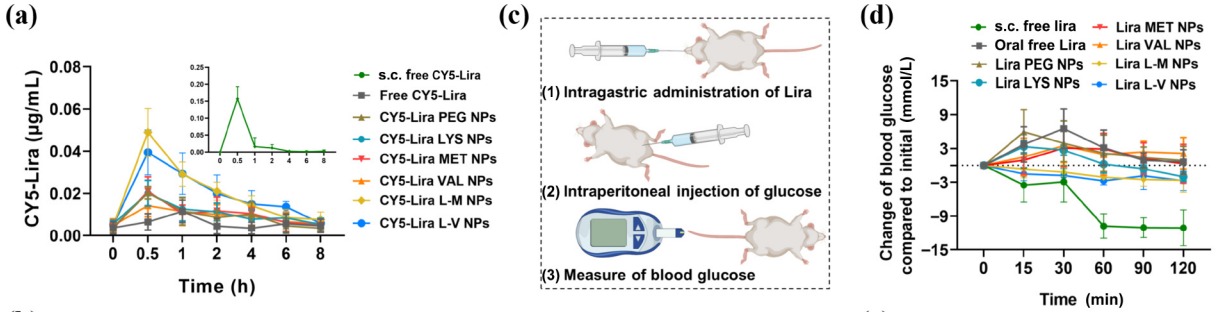

(b)

Sample	$AUC_{0-8\,h}$ (μg/(mL·h))	T_{MAX} (h)	C_{MAX} (μg/mL)	Fr (%)
s.c. free CY5-Lira	0.119 ± 0.023	0.5	0.157 ± 0.036	—
Free CY5-Lira	0.043 ± 0.020	1	0.012 ± 0.005	3.6 ± 1.7
CY5-Lira PEG NPs	0.066 ± 0.023^{ns}	0.5	0.020 ± 0.003*	5.5 ± 1.9^{ns}
CY5-Lira LYS NPs	0.074 ± 0.020*	0.5	0.020 ± 0.006*	6.2 ± 1.7*
CY5-Lira MET NPs	0.051 ± 0.042^{ns}	0.5	0.021 ± 0.007^{ns}	4.3 ± 3.5^{ns}
CY5-Lira VAL NPs	0.058 ± 0.031^{ns}	0.5	0.016 ± 0.005^{ns}	4.9 ± 2.6^{ns}
CY5-Lira L-M NPs	0.151 ± 0.029**	0.5	0.049 ± 0.011**	12.7 ± 2.5**
CY5-Lira L-V NPs	0.133 ± 0.031**	0.5	0.040 ± 0.011**	11.2 ± 2.6**

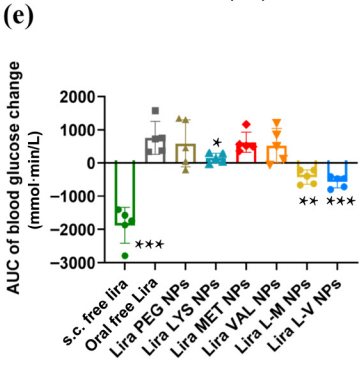

Figure 2 (a) Plasma CY5-Lira concentration–time profiles following the treatment of different formulations. (b) Pharmacokinetic parameters of CY5-Lira in mice. AUC: area under the curve of plasma CY5-Lira concentration versus time. Fr%: relative bioavailability. $^{*}p < 0.05$, $^{**}p < 0.01$, versus free CY5-Lira group. (c) Illustration of IPGTT which was conducted in type 2 diabetes db/db mice. (d) IPGTT profiles of type 2 diabetic db/db mice treated with different formulations. (e) AUC of IPGTT. Mean ± SD ($n = 5$). $^{*}p < 0.05$, $^{**}p < 0.01$, $^{***}p < 0.001$, versus oral free Lira group.

NPs markedly enhanced the oral drug delivery with Fr of 12.7% and 11.2%, respectively, which was about 3.3-fold higher than that of free CY5-Lira.

Postprandial blood glucose level (BGL) is a more accurate indicator of glycemic control compared to the fasting BGL [23]. Thus, the IPGTT [24] was conducted in type 2 diabetes db/db mice to further investigate the hypoglycemic activity of Lira-loaded NPs (Fig. 2(c)). The db/db mice were randomly grouped and administrated with different formulations. One hour later, 2 g/kg glucose was injected intraperitoneally and the BGL was monitored within 120 min (Figs. 2(d) and 2(e)). Thereinto, no hypoglycemic effect was observed after oral administration of free Lira and Lira PEG NPs. As for Lira MET/VAL NPs groups, although the maximum BGL was slightly reduced compared with free Lira group, their BGL was continually higher than the initial level throughout the experiment. In contrast, the BGL of Lira LYS NPs group was decreased to the initial level at 60 min and even 2 mmol/L lower than the initial value at 120 min. Compared with free Lira group, the AUC of Lira LYS NPs was reduced ($p < 0.05$) while Lira MET/VAL NPs had no significant difference ($p > 0.05$). Of note, oligopeptide-modified NPs (Lira L-M/L-V NPs) efficiently inhibited the rise in BGL and decreased the BGL below the initial value at 15 min, exhibiting a good ability in BGL control. Furthermore, oligopeptide-modified NPs showed a markedly reduced AUC, which was lower than zero, the AUC corresponding to the initial BGL.

Overall, the pharmacokinetic (PK) and pharmacodynamic (PD) results demonstrated that oligopeptide-modified NPs could effectively enhance the oral absorption of Lira, with superior performance in comparison with amino acid-modified NPs. In addition, by contrast with neutral amino acid-modified NPs (MET/VAL NPs), cationic amino acid-modified NPs (LYS NPs) exhibited superior oral delivery efficiency. Although all kinds of NPs showed good ability to protect Lira from enzymatic degradation *in vitro*, not all NPs could improve oral absorption of Lira *in vivo*. It hinted that the transepithelial barriers, including apical endocytosis, intracellular trafficking, and basolateral exocytosis of epithelium, might seriously hamper the efficacy of NPs *in vivo* [25–27]. Such differences might be related to the interactions between ligands and transporters [28, 29]. Hence, the influence of cationic amino acids, neutral amino acids, and oligopeptide modifications on the transepithelial behaviors of NPs needs to be further investigated.

3.4 Protein-based nutrients-functionalized NPs facilitated cellular uptake through the specific transporters

Mucus, covering the surface of the intestinal epithelium, is one of the main barriers to preclude most pharmaceutics. Orally administered nanoparticles have to overcome the mucus barrier before they get access to epithelial cells. Therefore, the mucus permeation ability of functionalized NPs was studied. The results indicated that compared with PEG NPs, the permeation of all ligand-modified NPs through mucus did not show significant changes (Fig. S4 in the ESM). Ligand modification had no influence on the mucus permeation ability of NPs. The cellular uptake of functionalized NPs was studied on Caco-2 cells (Fig. 3(a)). Compared with PEG NPs, the uptake of all kinds of ligand-modified NPs was promoted and their uptake gradually increased over time. Diverse ligands exhibited varying potencies. MET NPs showed the lowest uptake efficacy, which was 2.8-fold higher than that of PEG NPs at 2 h. It could be attributed to the relatively weak affinity between MET and neutral amino acid transporters. By contrast, other ligand-modified NPs demonstrated greater uptake ability, being 3.5–4.2 times higher than PEG NPs at 2 h.

Furthermore, the endocytosis mechanism of functionalized NPs was investigated. Competitive substrates of transporters were added during the process of NPs uptake. Free LYS, MET, and VAL inhibited the cellular uptake of LYS NPs, MET NPs, and VAL NPs, respectively, while that of PEG NPs was not affected (Figs. 3(b)–3(d)). GLY, the substrate of neutral amino acid transporters, suppressed the uptake of MET NPs and VAL NPs but had no effect on LYS NPs (Fig. 3(e)). The results indicated that cationic amino acid transporters were involved in the uptake of LYS NPs, while neutral amino acid transporters were responsible for the uptake of MET/VAL NPs.

Oligopeptides are formed through the covalent bonding of amino acids. It has been reported that oligopeptides are absorbed in the small intestine through PEPT1 [16]. Therefore, subsequent experiments were performed to explore the transporters involved in the uptake of oligopeptide-modified NPs. The involvement of amino acid transporters was first investigated. The results showed that free LYS and MET inhibited the uptake of L-M NPs (Fig. 3(f)). Similarly, free LYS and VAL also suppressed the uptake of L-V NPs. It indicated that amino acid transporters were still involved in the uptake of oligopeptide-modified NPs. On the other hand, Glysar, the substrate of PEPT1 [30], inhibited the uptake of L-M NPs and L-V NPs without affecting the uptake of PEG NPs (Fig. 3(g)), suggesting some certain relationship between oligopeptide-modified NPs with PEPT1. Furthermore, it was found that insulin, a regulatory molecule of PEPT1 [31], promoted the uptake of oligopeptide-modified NPs, while had no effect on the uptake of PEG NPs (Fig. 3(h)), thus further demonstrating the involvement of PEPT1 in the uptake of oligopeptide-modified NPs.

The expression of $b^{0,+}$AT (mediated cationic amino acid absorption), B^0AT1 (mediated neutral amino acid absorption), and PEPT1 on Caco-2 cells was further characterized by CLSM (Fig. S5 in the ESM). Compared with PEG NPs, LYS NPs, MET NPs, and L-M NPs increased the expression levels of $b^{0,+}$AT, B^0AT1, and PEPT1, respectively. And the three transporters exhibited the characteristic of polarity distribution, mainly distributed in the apical side of cells [19]. The results indicated that the expression of the three transporters was positively regulated by the corresponding ligand-modified NPs, which further contributed to the enhanced uptake.

3.5 Protein-based nutrients-functionalized NPs facilitated transepithelial transport

The transepithelial transport was further studied by the transwell model (Fig. 3(i)). Compared with PEG NPs, the permeation of all kinds of ligand-modified NPs through Caco-2 cell monolayers was promoted and different ligands exhibited varying degree of transepithelial transport properties. Among three amino acid-modified NPs, LYS NPs exhibited greater transepithelial transport efficiency than MET NPs and VAL NPs. Compared with the endocytosis, the exocytosis of MET NPs and VAL NPs was distinctly reduced. This suggested that in addition to the cellular uptake, the intracellular transport of NPs may also have an impact on the transmembrane efficiency [32]. Oligopeptide-modified NPs (L-M/L-V NPs) showed higher Papp values than those of amino acid-modified NPs and about 4.3-fold higher than those of PEG NPs.

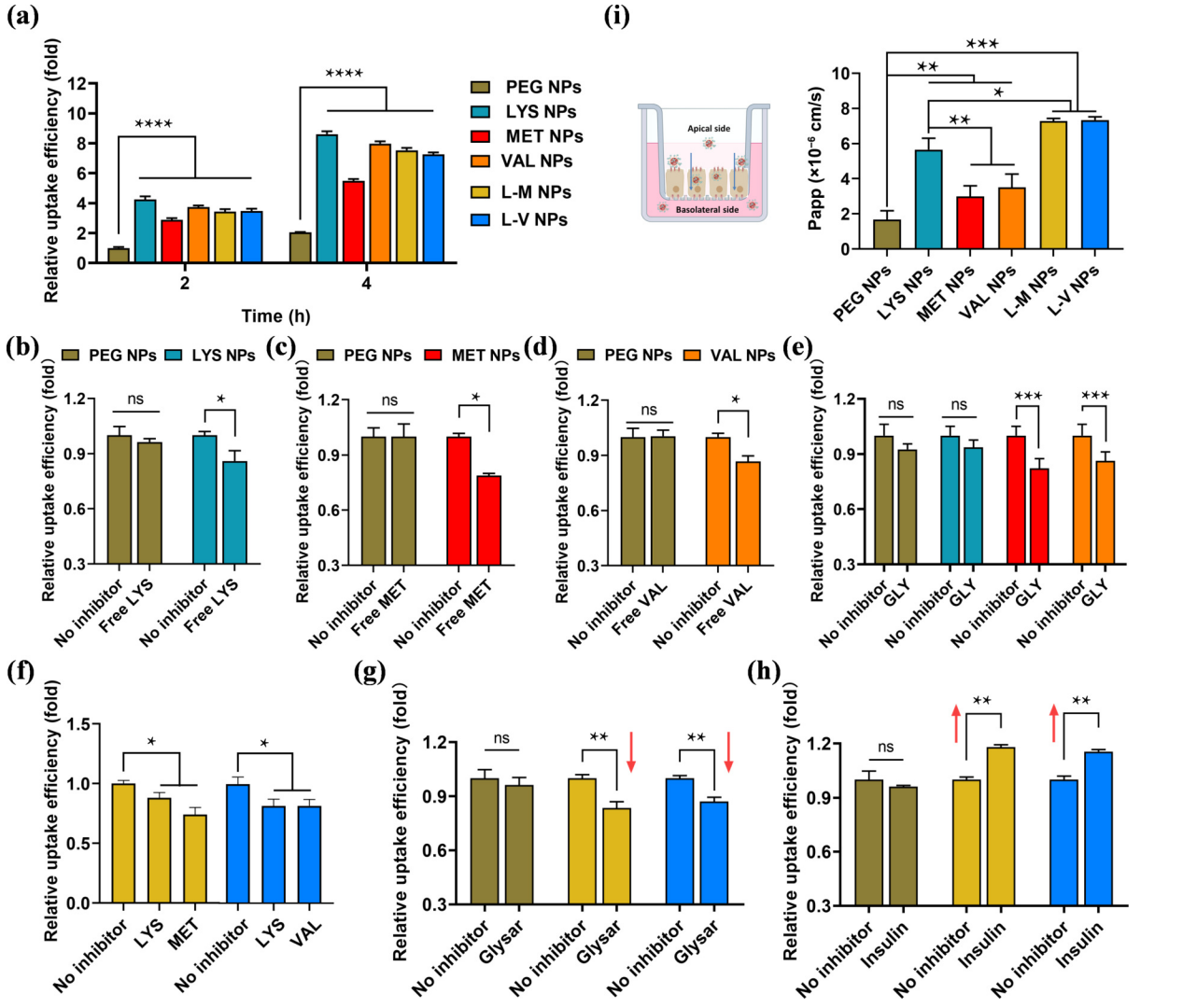

Figure 3 Endocytosis and transcytosis of NPs in Caco-2 cells. (a) The cellular uptake of NPs. (b)–(e) The effect of free amino acids on amino acids-modified NPs internalization. The effect of (f) free amino acids, (g) Glysar, and (h) insulin on oligopeptide-modified NPs internalization. (i) The Papp values of NPs during transport across Caco-2 cells. Mean ± SD ($n = 3$). *$p < 0.05$, **$p < 0.01$, ***$p < 0.001$, and ****$p < 0.0001$.

3.6 Protein-based nutrients functionalization changed the intracellular transport of NPs

To elucidate the intracellular transport, we investigated the impact of specific inhibitors on the exocytosis of NPs (Fig. 4(a)). LY294002, Brefeldin A, and Monensin were used to inhibit the lysosome transport, the endoplasmic reticulum (ER)-Golgi pathway, and the Golgi-plasma membrane pathway, respectively. The results showed that LY294002 and Brefeldin A significantly enhanced the intracellular accumulation of PEG NPs while Monensin did not cause significant changes, suggesting the involvement of lysosome and endoplasmic reticulum pathway in the intracellular transport. MET and VAL-functionalization had no influence on the intracellular transport of PEG NPs. By contrast, LYS, L-M, and L-V-functionalization changed the intracellular fate of NPs. Monensin significantly increased the intracellular retention of LYS NPs, while LY294002 and Brefeldin A had no effect on it, indicating that LYS NPs were mainly transported through the Golgi apparatus rather than the lysosome and endoplasmic reticulum. In addition, the exocytosis of L-M NPs and L-V NPs was inhibited by Monensin and Brefeldin A but not by LY294002. This suggested that L-M NPs and L-V NPs could escape from lysosomes and were primarily transported through the endoplasmic reticulum and Golgi apparatus. Furthermore, the colocalization of NPs with organelles was directly observed by CLSM (Fig. 4(b)). The semi-quantitative results were generally in agreement with the above results using specific inhibitors.

In summary, MET NPs and VAL NPs were mainly transported through lysosomes and endoplasmic reticulum, and their transmembrane transport efficiency was relatively low due to the degradation in lysosomes. Compared to MET NPs and VAL NPs, LYS NPs not only enhanced the Golgi apparatus pathway, facilitating exocytosis, but also avoided the lysosomal pathway, reducing intracellular degradation. Consequently, the transmembrane transport efficiency was significantly improved. Interestingly, the intracellular transport of oligopeptide-modified NPs perfectly combined the characteristics of LYS NPs and MET/VAL NPs, involving endoplasmic reticulum and Golgi apparatus but excluding lysosomes (Fig. 4(c)). Additionally, the mechanism of LYS NPs and oligopeptide-modified NPs escaping from lysosomes was further explored. The zeta potentials of NPs were measured at pH 5.5, which simulated the acidic environment

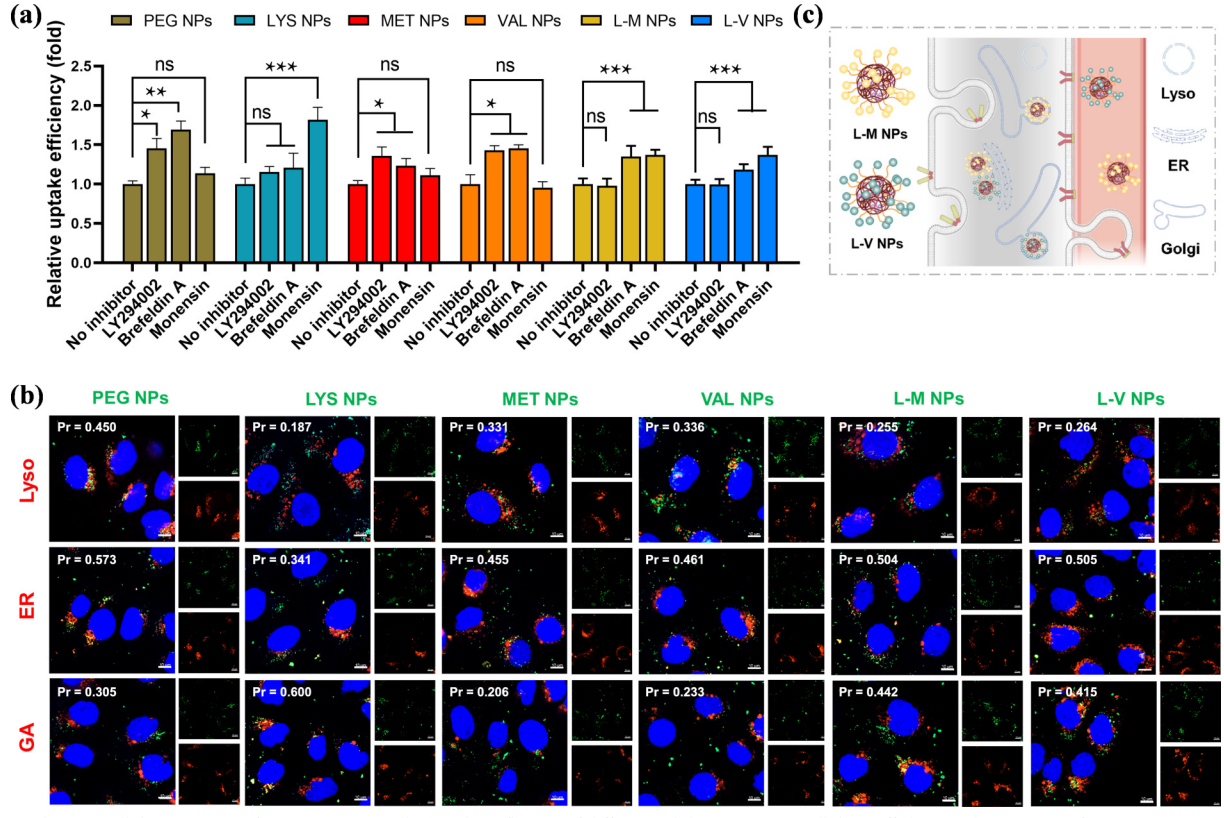

Figure 4 The intracellular transport of NPs in Caco-2 cells. (a) The influence of different inhibitors on intracellular trafficking and exocytosis of NPs. Mean ± SD (n = 3). *p < 0.05, **p < 0.01, and ***p < 0.001. (b) Representative CLSM images of the colocalization of NPs with Lysosomes, ER, and Golgi in Caco-2 cells. Bule: cell nucleus, green: FITC-Lira-loaded NPs, and red: organell. Scale bar = 10 μm. (c) The schematic graph of oligopeptide-modified NPs intracellular transport.

within lysosomes (Fig. S6 in the ESM). LYS NPs and oligopeptide-modified NPs were positively charged at pH 5.5 because of the protonation of amine groups, which might contribute to escaping lysosomes by the proton sponge effect [33, 34].

In vitro cell experiments showed that NPs modified with different ligands exhibited varying transmembrane transport efficiency. Cationic amino acid-modified NPs exhibited superior transmembrane transport efficiency compared to neutral amino acid-modified NPs, which was consistent with the *in vivo* findings. Of note, the *in vitro* transmembrane transport efficiency of oligopeptide-modified NPs was only 1.2-fold higher than LYS NPs. However, a significant difference in drug delivery efficiency was observed *in vivo*, with the Fr of oligopeptide-modified NPs approximately twice as high as that of LYS NPs. In addition, MET NPs and VAL NPs showed certain advantages in cellular uptake and transmembrane transport compared with PEG NPs *in vitro*, but in pharmacodynamic and pharmacokinetic evaluation, they barely showed enhanced absorption effects. Such contradictions between the *in vitro* and *in vivo* findings suggested that, in addition to the interaction between ligands and transporters, there might be other factors that influenced the drug delivery efficiency of ligand-modified NPs *in vivo*.

3.7 Lysine and oligopeptide-functionalization affected the absorption site of NPs in intestine

In order to reveal the above mentioned contradictions, we further investigated the absorption and transmembrane transport of NPs in different intestinal segments, comprehensively studying the absorption characteristics throughout the small intestine. *In situ* ligated intestinal loop model demonstrated that the absorption of PEG NPs, MET NPs, and VAL NPs was all negligible throughout the small intestine, which was consistent with *in vivo* results (Fig. 5(a)). LYS NPs, L-M NPs, and L-V NPs showed enhanced absorption compared to PEG NPs. Interestingly, the absorption of LYS NPs was lower in the duodenum and jejunum, but significantly higher in the ileum. In contrast, the absorption of L-M NPs and L-V NPs occurred primarily in the duodenum and jejunum with less absorption occurring in the ileum. The difference of absorption site between LYS NPs and oligopeptide-modified NPs was further confirmed by *ex vivo* intestinal model (Fig. 5(b)). Compared to PEG NPs, the Papp values of LYS NPs, L-M NPs, and L-V NPs were increased in all intestinal segments. Additionally, the quantitative results were consistent with the qualitative trends. LYS NPs exhibited the highest transmembrane transport efficiency in the ileum, whereas the Papp values of L-M NPs and L-V NPs decreased from duodenum to jejunum and finally to ileum.

The different absorption sites of LYS NPs and oligopeptide-modified NPs might be attributed to the spatial distribution of transporters in the small intestine. The expression of $b^{0,+}$AT and PEPT1 on different intestinal segments was characterized by CLSM (Fig. 5(c)). In contrast to the duodenum and jejunum, the ileum exhibited the highest expression level of $b^{0,+}$AT. Conversely, the expression level of PEPT1 gradually decreased from duodenum to jejunum, then to ileum. These results demonstrated that LYS NPs were primarily absorbed in the distal small intestine mediated by $b^{0,+}$AT, whereas oligopeptide-modified NPs were primarily absorbed in the proximal small intestine mediated by PEPT1 (Fig. 5(d)). Based on the absorption characteristics of proteins, pancreatic

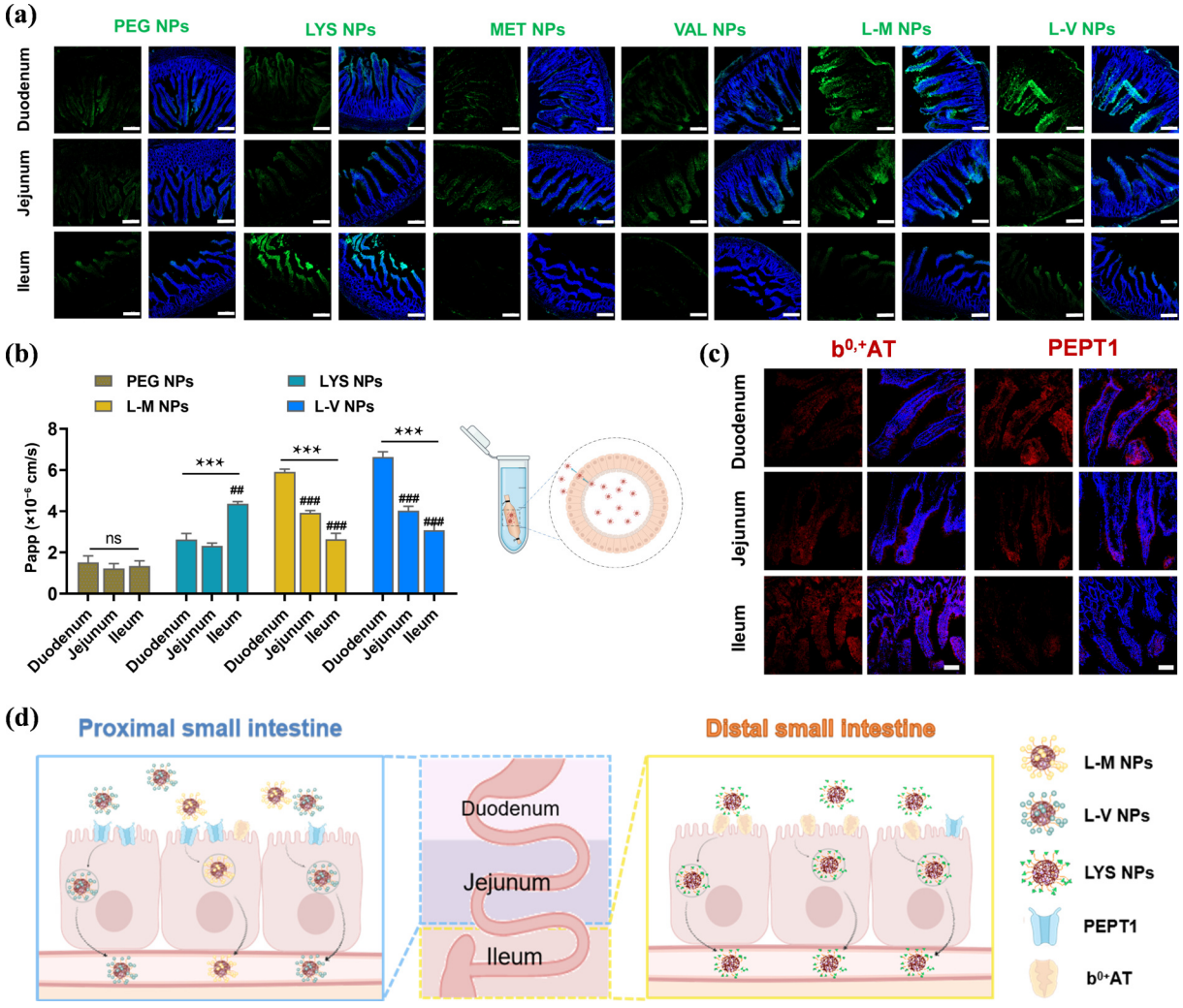

Figure 5 (a) CLSM images of NPs *in situ* absorption in various intestinal segments (duodenum, jejunum, and ileum). Blue: intestinal epithelial nucleus, and green: FITC-Lira-loaded NPs. Scale bar = 200 μm. (b) The Papp values of NPs penetrating the *ex vivo* duodenum, jejunum, and ileum sections. Mean ± SD (n = 3). ***p < 0.001, versus PEG NPs. ##p < 0.01 and ###p < 0.001 compared to duodenum. (c) Immunofluorescence staining of $b^{0,+}$AT and PEPT1 in the small intestine. Blue: intestinal epithelial nucleus, and red: $b^{0,+}$AT or PEPT1. Scale bar = 100 μm. (d) Illustration of the absorption processes of LYS NPs and oligopeptide-modified NPs in different sites of small intestine.

proteases digest proteins into large peptides, and then membrane-bound peptidases further break down into oligopeptides, finally formed absorbable amino acids [35, 36]. These peptidases are present throughout the small intestine but are more active in the ileum than in the jejunum [37]. Consequently, as contents move from the duodenum to the ileum, free amino acid levels increase, while oligopeptide concentrations decrease [19]. So the differential gradients in the expression for $b^{0,+}$AT and PEPT1 along the jejuno-ileal axis might exhibited physiological relevance that favored the absorption of protein-based nutrients.

It was possible that the spatial distribution of transporters also affected the drug delivery efficiency of NPs *in vivo*. Luminal trypsin exhibited high activity throughout the small intestine [38–40]. Due to the low expression of $b^{0,+}$AT in the proximal small intestine, LYS NPs had to migrate to the ileum to be efficiently absorbed into the bloodstream. This process might result in much more Lira being enzymatically degraded before reaching the ileum, ultimately leading to the limited drug absorption. In contrast, L-M NPs and L-V NPs were mainly absorbed in the proximal small intestine, which could help to reduce the enzymatic degradation of Lira and thus achieve superior oral absorption effect. Furthermore, the proximal small intestine, as the primary site for the digestion and absorption of nutrients, has a large absorption area and abundant blood vessels, thereby exhibiting a formidable absorption capacity [41–43]. Therefore, the high expression of PEPT1 in the proximal small intestine favored efficient absorption of L-M NPs and L-V NPs. This suggested that the spatial distribution of transporters might also be an important factor to be considered in the design of ligand-modified nanoparticles.

3.8 Oligopeptide-modified NPs controlled blood glucose level of diabetes during the long-term therapy

To further evaluate the long-term therapeutic efficacy of Lira-loaded NPs, the diabetic mice were orally administered with free Lira, Lira PEG NPs, Lira LYS NPs, Lira L-M NPs, and Lira L-V NPs, respectively, once a day for 28 days. The FBG was recorded every four days (Fig. 6(a)). Subcutaneous injection of Lira dramatically decreased the FBG, while the FBG in oral free Lira, Lira PEG NPs, and Lira LYS NPs groups continuously increased (Fig. 6(b)). By comparison, oral administration of Lira L-M NPs

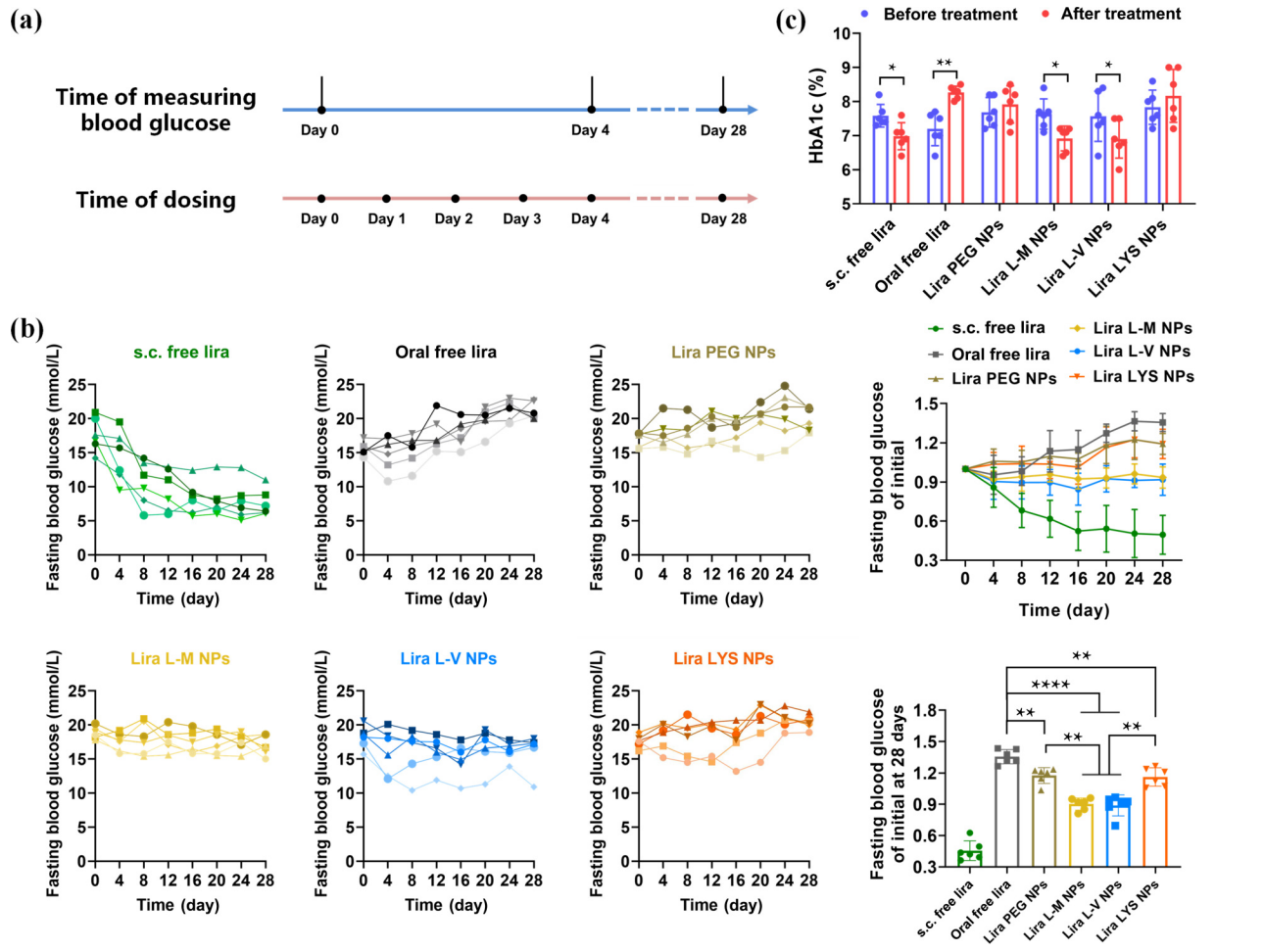

Figure 6 (a) Schedule diagram of long-term treatment in db/db mice. The mice were given dosage once a day, and the fasting blood-glucose were recorded every four days. (b) Fasting blood glucose of db/db mice with long-term treatment. (c) HbA1c of db/db mice before and after long-term treatment. Mean ± SD (n = 6). *p < 0.05, **p < 0.01, ***p < 0.001, and ****p < 0.0001.

and Lira L-V NPs effectively inhibited the rise of FBG and could maintain FBG during 28 days, demonstrating the good ability in FBG control. Moreover, HbA1c, which was produced through the irreversible binding of blood glucose with hemoglobin and served as a crucial indicator for long-term blood glucose level control [44, 45], was measured before and after 28 days treatment (Fig. 6(c)). Lira L-M/L-V NPs successfully lowered the HbA1c levels to about 7%. Surprisingly, orally administered Lira L-M/L-V NPs exhibited comparable hypoglycemic effects of s.c. free Lira. These results demonstrated that oligopeptide-modified NPs could effectively control blood glucose level of type 2 diabetes during the long-term therapy, which might be beneficial for preventing diabetes complications.

3.9 Oligopeptide-modified NPs alleviated symptoms of diabetes after long-term treatment

The pancreatic β-cells play a crucial role in systemic metabolism by secreting insulin, the sole hormone in the body that reduces plasma glucose levels [46, 47]. The pancreatic α-cells regulate blood glucose by secreting glucagon [48]. Type 2 diabetes is characterized by the progressive damage of pancreatic β-cells function and insulinopenia, and by the disrupted glucagon secretion from pancreatic α-cells [49, 50]. Lira, a glucagon-like peptide-1 (GLP-1) receptor agonist, is able to promote the β-cells repair and proliferation [51]. Herein, the immunofluorescence staining of insulin and glucagon was conducted to assess the amount and function of α-cells and β-cells (Fig. 7(a)). For the s.c. free Lira and oral Lira L-M/L-V NPs groups, β-cells accounted for a high proportion and were widely distributed across the islets, whereas α-cells were scarce and mainly confined to the islet periphery, resembling the islets of healthy mice [52]. By contrast, the proportion of β-cells in the oral free Lira, Lira PEG NPs, and Lira LYS NPs groups was reduced, while the proportion of α-cells was increased and diffused towards the interior of the islets, indicating the occurrence of islet lesions. Meanwhile, the morphologic analysis of pancreas was conducted via H&E staining (Fig. 7(b)). Obvious islet lesions were observed in oral free Lira and Lira PEG NPs groups, while alleviated lesions were observed in Lira LYS NPs group. Notably, Lira L-M/L-V NPs groups exhibited similar characteristics to those of s.c. free Lira group, featuring a large number of islets with mostly circular distribution and clear structural boundaries. In general, it was demonstrated that Lira L-M/L-V NPs could effectively repair islet damage caused by long-term hyperglycemia, almost reaching the same level as the s.c. free Lira. In addition, the blood insulin level, reflecting the function of pancreatic β-cells, was measured (Fig. 7(c)). Compared to oral free Lira group, Lira L-M/L-V NPs significantly increased insulin concentrations (p < 0.01), whereas Lira PEG NPs and Lira LYS NPs showed no difference (p > 0.05).

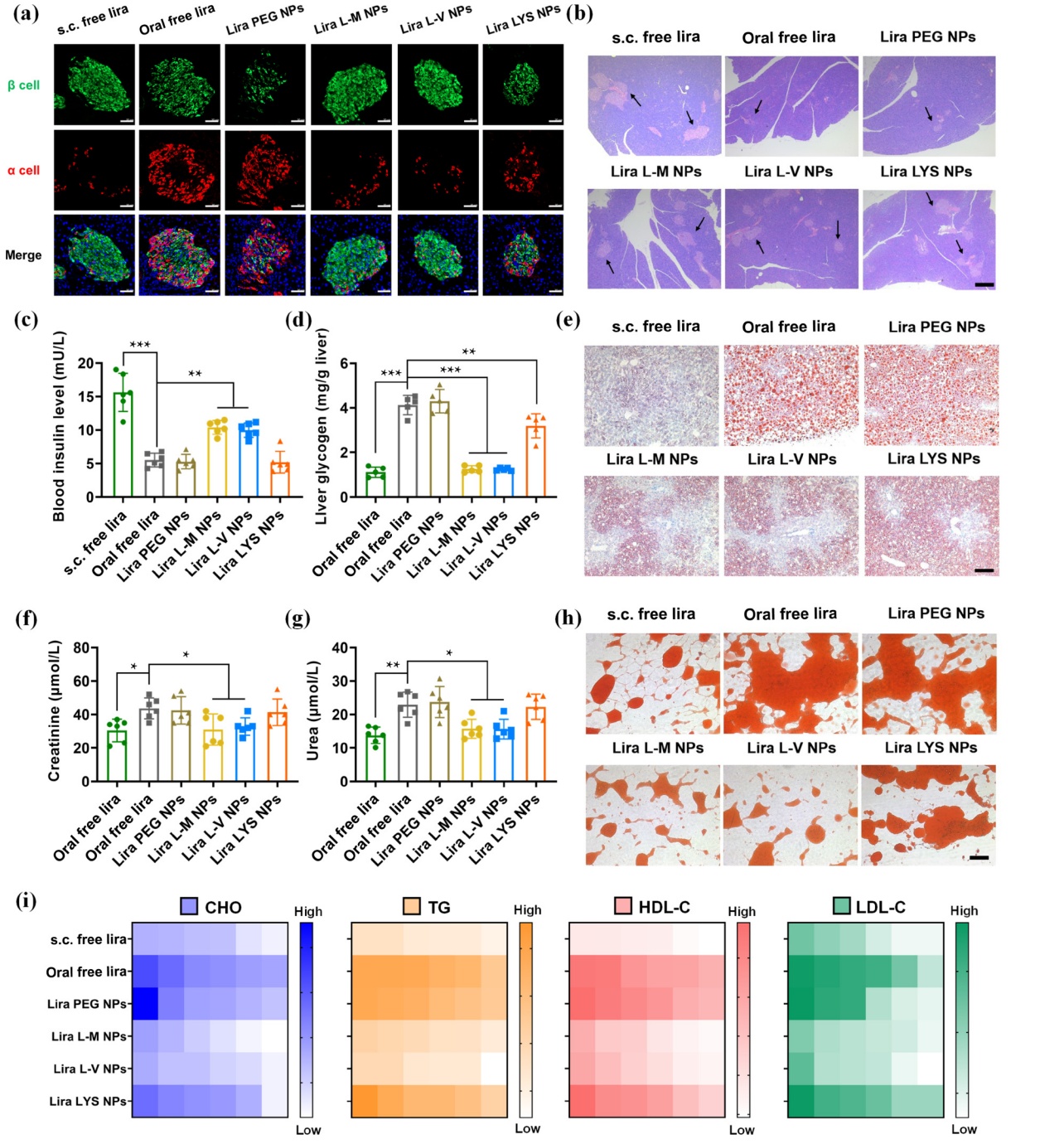

Figure 7 Pharmacodynamic evaluation of pancreas, liver, and serum lipid after long-term treatment in db/db mice. (a) Representative images of immunofluorescent staining of pancreas islets. Green: β cell, red: α cell, and bule: cell nucleus. Scale bar = 50 μm. (b) Representative images of H&E staining of pancreas. Scale bar = 400 μm. (c) Blood insulin level after long-term treatment. (d) Liver glycogen after long-term treatment. (e) Representative images of oil red O staining of liver. Scale bar = 200 μm. (f) Blood creatinine after long-term treatment. (g) Blood urea after long-term treatment. (h) Representative images of oil red O staining of epididymal visceral adipose tissue. Scale bar = 200 μm. (i) CHO, TG, HDL-C, and LDL-C after long-term treatment. Mean ± SD ($n = 6$). *$p < 0.05$, **$p < 0.01$, and ***$p < 0.001$.

The liver plays an important role in energy homeostasis and glucose metabolism. Generally, insulin enhances glycogen synthesis in the liver and prevents glucose production. However, these normal physiologic processes become dysregulated with type 2 diabetes mellitus, leading to increased free fatty acids, thus causing increased hepatic gluconeogenesis [53, 54]. The liver glycogen level was measured before and after the long-term treatment. Lira LYS/L-M/L-V NPs dramatically decreased glycogen level of db/db mice compared with oral free Lira group (Fig. 7(d)). Of note, Lira L-M/L-V NPs groups showed a similar glycogen level with s.c. free Lira group ($p > 0.05$). The liver histological morphology was assessed by Oil red O staining. The results showed that a large amount of fat deposition in liver was observed in oral free Lira group, while alleviated fat deposition was observed in Lira LYS/L-M/L-V NPs groups (Fig. 7(e)). Creatinine and urea levels are observed to be increased in diabetic mice due to the abnormal renal

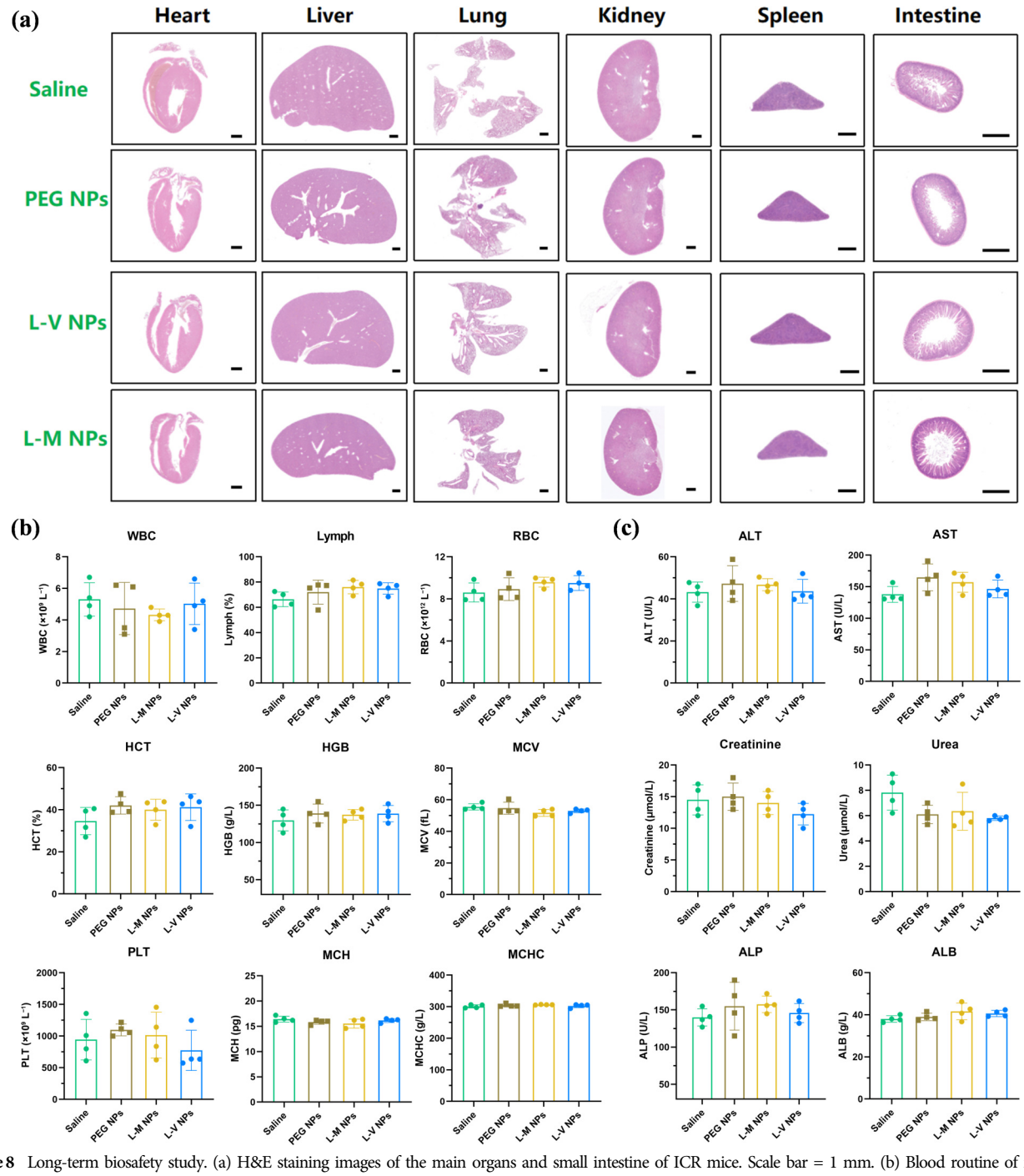

Figure 8 Long-term biosafety study. (a) H&E staining images of the main organs and small intestine of ICR mice. Scale bar = 1 mm. (b) Blood routine of mice in different groups. WBC: white blood cells, Lym: lymphocyte, RBC: red blood cells, HGB: hemoglobin, HCT: hematocrit, MCV: mean cell volume, PLT: blood platelet, MCH: mean corpuscular hemoglobin, and MCHC: mean corpuscular hemoglobin concentration. (c) Biochemistry tests of mice in different groups. ALT: alanine transferase, AST: aspartate transferase, ALP: alkaline phosphatase, and ALB: albumin. Mean ± SD (n = 4).

function [55]. After 28 days of treatment, Lira L-M/L-V NPs remarkably reduced the creatinine and urea levels and exhibited almost the same effect as the s.c. free Lira (Figs. 7(f) and 7(g)).

In addition, epididymal white adipose tissue was collected and stained with Oil red O to directly observe the morphology of fat tissue (Fig. 7(h)). Lira LYS NPs group showed less fat content compared to oral free Lira and Lira PEG NPs groups. Lira L-M/L-V NPs markedly decreased the fat content of adipose tissue, and the therapeutic effect was similar to s.c. group. Type 2 diabetes frequently has a complication of dyslipidemia [56]. Therefore, plasma lipid parameters including CHO, TG, HDL-C, and LDL-C were measured after 28 days of drug administration (Fig. 7(i) and Fig. S7 in the ESM). Compared with the oral free Lira group, s.c. free Lira and Lira L-M/L-V NPs dramatically decreased CHO, TG, HDL-C and LDL-C levels ($p < 0.001$). However, Lira PEG/LYS NPs had no significant difference with oral free Lira ($p > 0.05$).

These results indicated that long-term treatment of Lira LYS NPs only showed a certain therapeutic effect on some indicators in

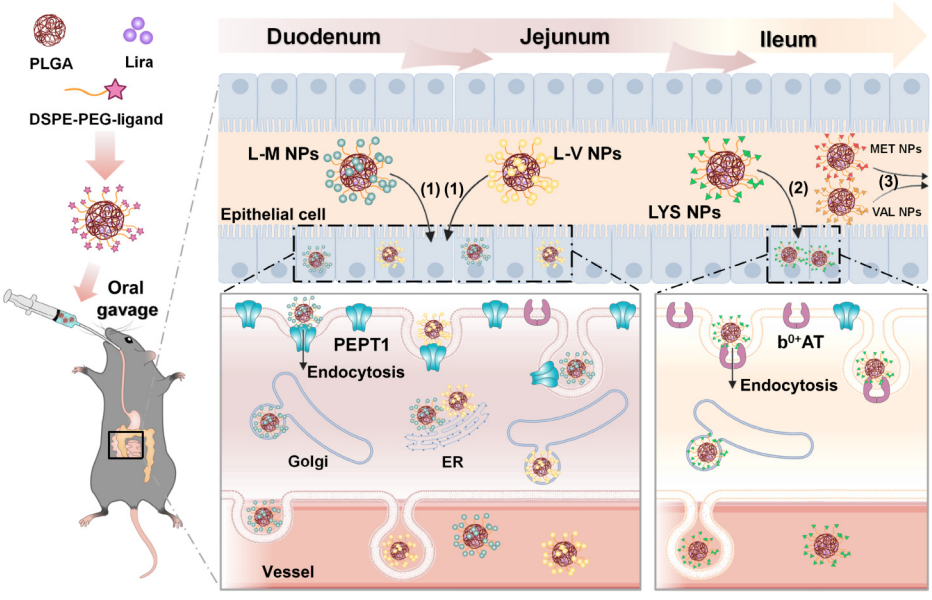

Figure 9 Schematic illustration for the oral absorption process and mechanism of protein-based nutrients-functionalized NPs. (1) Oligopeptide-modified NPs (L-M NPs and L-V NPs) were primarily absorbed in the duodenum and jejunum, mediated by PEPT1, which favored the absorption of Lira. Endoplasmic reticulum and Golgi apparatus were involved in the intracellular transport. (2) Cationic amino acid-modified NPs (LYS NPs) were mainly absorbed in the ileum, mediated by $b^{0,+}$AT, which was unfavourable for the stability of Lira, thus leading to limited absorption. (3) Neutral amino acid-modified NPs (MET NPs and VAL NPs) were poorly absorbed throughout the small intestine.

db/db mice. In contrast, oligopeptide-modified NPs exhibited superior long-term treatment effect. They could effectively control the blood glucose level, reduce plasma lipid level, and repair tissue damage in type 2 diabetic mice. It should be noted that oligopeptide-modified NPs exhibited almost the same therapeutic effects as the s.c. free Lira in many indexes, including HbA1c, liver glycogen, creatinine, urea, CHO, TG, and so on. Overall, oral drug delivery system mimicking oligopeptide absorption route demonstrated significantly predominant in drug delivery efficiency compared to that of amino acid absorption route. This could be attributed primarily to two major reasons. Firstly, oligopeptide-modified NPs significantly promoted the cellular uptake and transcytosis in intestinal epitheliums by mediation of PEPT1. Secondly, NPs modified with amino acids and oligopeptides exhibited varying absorption sites of the small intestine. Amino acids-modified NPs were mainly absorbed in the distal small intestine, whereas oligopeptide-modified NPs were primarily absorbed in the proximal small intestine due to the difference in the spatial distribution of transporters. The rapid absorption of NPs in the proximal small intestine might be more conducive to keeping the drug intact, thereby achieving superior oral absorption.

3.10 Oligopeptide-modified NPs exhibited good biosafety

For the safety concerns, the long-term safety of daily oral administration of normal saline, PEG NPs, L-M NPs, and L-V NPs for 28 days in mice was studied. The histology analysis revealed that no obvious pathological alterations and abnormal inflammatory responses were detected in the small intestine and other vital organs (heart, liver, spleen, lung, and kidney) of each group (Fig. 8(a) and Fig. S8 in the ESM). Furthermore, the blood routine and blood biochemistry index of the NPs-treated groups did not exhibit significant changes compared with the control group (Figs. 8(b) and 8(c)). The results indicated that oligopeptide-modified NPs had good biocompatibility.

4 Conclusions

In summary, inspired by the natural and efficient absorption of protein-based nutrients in intestine, we developed several kinds of oral drug delivery systems to simulate the absorption of amino acids or oligopeptides (Fig. 9). All kinds of functionalized NPs showed enhanced cellular uptake and transepithelial transport mediated by specific transporters *in vitro*. Through reducing degradation by lysosomes and promoting Golgi apparatus transport, oligopeptide-modified NPs exhibited higher transepithelial transport efficiency than amino acid-modified NPs. *In vivo* study showed that oligopeptide-modified NPs significantly improved the oral bioavailability of Lira compared to amino acid-modified NPs, which might be due to the different absorption sites in intestine. Moreover, oral administration of oligopeptide-modified Lira-loaded NPs exhibited good abilities in glucose control, reduction of plasma lipid level, and alleviation of organ lesions in long-term treatment of diabetic mice. Overall, compared with amino acid, oligopeptide-simulated oral drug delivery system was more suitable for oral drug delivery. Additionally, this study also revealed that the spatial distribution of transporters might influence the drug delivery efficiency of ligand-modified nanocarriers. The natural oligopeptide absorption-mimicking oral drug delivery systems exhibit efficient delivery behavior and good biocompatibility, showing promising application potential in the treatment of chronic diseases requiring long-term medication.

Electronic Supplementary Material: Supplementary material (^{1}H-NMR spectra of materials, FTIR spectra of materials, the size, zeta potential, EE, and DL of nanoparticles, Papp values of NPs during transport across mucus, CLSM images of $b^{0,+}$AT, B^0AT1, and PEPT1 in Caco-2 cells, zeta potential of nanoparticles at pH 5.5, plasma lipid parameters after long-term treatment, and H&E staining images of the main organs and small intestine after long-term biosafety study) is available in the online version of this article at https://doi.org/10.26599/NR.2025.94907082.

Data availability

All data needed to support the conclusions in the paper are presented in the manuscript and the Electronic Supplementary Material. Additional data related to this paper may be requested from the corresponding author upon request.

Acknowledgements

This work was supported by the National Key Research and Development Program of China (No. 2021YFE0115200) and the Regional Innovation and Development Joint Fund of National Natural Science Foundation of China (No. U22A20356).

Declaration of competing interest

All the contributing authors report no conflict of interests in this work.

Author contribution statement

R. N. W.: Methodology, formal analysis, validation, conceptualization, data curation. X. X. F.: Methodology, formal analysis, visualization, investigation, writing – original draft, writing – review & editing. L. C. W.: Resources, investigation, methodology. L. Y. X.: Resources, formal analysis. J. X. K.: Resources, formal analysis. Z. Z.: Writing – review & editing. J. Y. W.: Writing – review & editing. L. L.: Project administration, writing – review & editing. Y. H.: Funding acquisition, supervision, conceptualization, project administration, writing – review & editing. All the authors have approved the final manuscript.

Informed consent

Not applicable.

Ethics statement

The animal experiments were carried out following the guidelines of the Sichuan University Institutional Committee for the Care and Use of Laboratory Animals and were approved by the Medical Ethics Committee of Sichuan University (ethical code: SYXK(Chuan)2018–113).

Use of AI statement

None.

References

[1] Ji, W.; Zhang, P.; Zhou, Y. G.; Zhou, X. Q.; Ma, X. F.; Tan, T. W.; Cao, H. Hydrogel-encapsulated medium chain lipid-modified zeolite imidazole framework-90 as a promising platform for oral delivery of proteins. *J. Control. Release* **2024**, *367*, 93–106.

[2] Wu, R. N.; Wu, Z. H.; Xing, L. Y.; Liu, X.; Wu, L.; Zhou, Z.; Li, L.; Huang, Y. Mimicking natural cholesterol assimilation to elevate the oral delivery of liraglutide for type II diabetes therapy. *Asian J. Pharm. Sci.* **2022**, *17*, 653–665.

[3] Anselmo, A. C.; Gokarn, Y.; Mitragotri, S. Non-invasive delivery strategies for biologics. *Nat. Rev. Drug Discov.* **2019**, *18*, 19–40.

[4] Drucker, D. J. Advances in oral peptide therapeutics. *Nat. Rev. Drug Discov.* **2020**, *19*, 277–289.

[5] Abeer, M. M.; Rewatkar, P.; Qu, Z.; Talekar, M.; Kleitz, F.; Schmid, R.; Lindén, M.; Kumeria, T.; Popat, A. Silica nanoparticles: A promising platform for enhanced oral delivery of macromolecules. *J. Control. Release* **2020**, *326*, 544–555.

[6] Han, Y.; Gao, Z. G.; Chen, L. Q.; Kang, L.; Huang, W.; Jin, M. J.; Wang, Q. M.; Bae, Y. H. Multifunctional oral delivery systems for enhanced bioavailability of therapeutic peptides/proteins. *Acta Pharm. Sin. B* **2019**, *9*, 902–922.

[7] Brayden, D. J.; Alonso, M. J. Oral delivery of peptides: Opportunities and issues for translation. *Adv. Drug Deliv. Rev.* **2016**, *106*, 193–195.

[8] Haddadzadegan, S.; Dorkoosh, F.; Bernkop-Schnürch, A. Oral delivery of therapeutic peptides and proteins: Technology landscape of lipid-based nanocarriers. *Adv. Drug Deliv. Rev.* **2022**, *182*, 114097.

[9] Have, G. A. M. T.; Engelen, M. P. K. J.; Luiking, Y. C.; Deutz, N. E. P. Absorption kinetics of amino acids, peptides, and intact proteins. *Int. J. Sport Nutr. Exerc. Metab.* **2007**, *17*, S23–S36.

[10] Trommelen, J.; Tomé, D.; van Loon, L. J. C. Gut amino acid absorption in humans: Concepts and relevance for postprandial metabolism. *Clin. Nutr. Open Sci.* **2021**, *36*, 43–55.

[11] Adibi, S. A.; Gray, S. J.; Menden, E. The kinetics of amino acid absorption and alteration of plasma composition of free amino acids after intestinal perfusion of amino acid mixtures. *Am. J. Clin. Nutr.* **1967**, *20*, 24–33.

[12] Bröer, S.; Fairweather, S. J. Amino acid transport across the mammalian intestine. *Compr. Physiol.* **2019**, *9*, 343–373.

[13] Loveday, S. M. Protein digestion and absorption: The influence of food processing. *Nutr. Res. Rev.* **2023**, *36*, 544–559.

[14] Bröer, S.; Gauthier-Coles, G. Amino acid homeostasis in mammalian cells with a focus on amino acid transport. *J. Nutr.* **2022**, *152*, 16–28.

[15] Xia, R.; Peng, H. F.; Zhang, X.; Zhang, H. S. Comprehensive review of amino acid transporters as therapeutic targets. *Int. J. Biol. Macromol.* **2024**, *260*, 129646.

[16] Spanier, B.; Rohm, F. Proton coupled oligopeptide transporter 1 (PepT1) function, regulation, and influence on the intestinal homeostasis. *Compr. Physiol.* **2018**, *8*, 843–869.

[17] Bröer, S. Amino acid transport across mammalian intestinal and renal epithelia. *Physiol. Rev.* **2008**, *88*, 249–286.

[18] Bröer, S.; Bröer, A. Amino acid homeostasis and signalling in mammalian cells and organisms. *Biochem. J.* **2017**, *474*, 1935–1963.

[19] Bhutia, Y. D.; Ganapathy, V. Protein digestion and absorption. In *Physiology of the Gastrointestinal Tract*, 6th ed. Said, H. M., Ed.; Elsevier: Amsterdam, 2018; pp 1063–1086.

[20] Wu, L.; Liu, M.; Shan, W.; Zhu, X.; Li, L. J.; Zhang, Z. R.; Huang, Y. Bioinspired butyrate-functionalized nanovehicles for targeted oral delivery of biomacromolecular drugs. *J. Control. Release* **2017**, *262*, 273–283.

[21] Wu, L. C.; Xing, L. Y.; Wu, R. N.; Fan, X. X.; Ni, M. J.; Xiao, X.; Zhou, Z.; Li, L.; Wen, J. Y.; Huang, Y. Lipoic acid-mediated oral drug delivery system utilizing changes on cell surface thiol expression for the treatment of diabetes and inflammatory diseases. *J. Mater. Chem. B* **2024**, *12*, 3970–3983.

[22] Wu, L.; Bai, Y. L.; Wang, L. L.; Liu, X.; Zhou, R.; Li, L.; Wu, R. N.; Zhang, Z. R.; Zhu, X.; Huang, Y. Promoting apical-to-basolateral unidirectional transport of nanoformulations by manipulating the nutrient-absorption pathway. *J. Control. Release* **2020**, *323*, 151–160.

[23] Avignon, A.; Radauceanu, A.; Monnier, L. Nonfasting plasma glucose is a better marker of diabetic control than fasting plasma glucose in type 2 diabetes. *Diabetes Care* **1997**, *20*, 1822–1826.

[24] Small, L.; Ehrlich, A.; Iversen, J.; Ashcroft, S. P.; Trošt, K.; Moritz, T.; Hartmann, B.; Holst, J. J.; Treebak, J. T.; Zierath, J. R. et al. Comparative analysis of oral and intraperitoneal glucose tolerance tests in mice. *Mol. Metab.* **2022**, *57*, 101440.

[25] Yu, M. R.; Yang, Y. W.; Zhu, C. L.; Guo, S. Y.; Gan, Y. Advances in the transepithelial transport of nanoparticles. *Drug Discov. Today* **2016**, *21*, 1155–1161.

[26] Xi, Z. Y.; Ahmad, E.; Zhang, W.; Li, J. Y.; Wang, A. H.; Faridoon; Wang, N.; Zhu, C. L.; Huang, W.; Xu, L. et al. Dual-modified

nanoparticles overcome sequential absorption barriers for oral insulin delivery. *J. Control. Release* **2022**, *342*, 1–13.
[27] Xu, Y. N.; Zheng, Y. X.; Wu, L.; Zhu, X.; Zhang, Z. R.; Huang, Y. Novel solid lipid nanoparticle with endosomal escape function for oral delivery of insulin. *ACS Appl. Mater. Interfaces* **2018**, *10*, 9315–9324.
[28] Yun, Y.; Cho, Y. W.; Park, K. Nanoparticles for oral delivery: Targeted nanoparticles with peptidic ligands for oral protein delivery. *Adv. Drug Deliv. Rev.* **2013**, *65*, 822–832.
[29] Pangeni, R.; Kang, S.; Jha, S. K.; Subedi, L.; Park, J. W. Intestinal membrane transporter-mediated approaches to improve oral drug delivery. *J. Pharm. Investig.* **2021**, *51*, 137–158.
[30] Du, Y. Q.; Tian, C. T.; Wang, M. L.; Huang, D.; Wei, W.; Liu, Y.; Li, L.; Sun, B. J.; Kou, L. F.; Kan, Q. M. et al. Dipeptide-modified nanoparticles to facilitate oral docetaxel delivery: New insights into PepT1-mediated targeting strategy. *Drug Deliv.* **2018**, *25*, 1403–1413.
[31] Watanabe, K.; Terada, K.; Jinriki, T.; Sato, J. Effect of insulin on cephalexin uptake and transepithelial transport in the human intestinal cell line Caco-2. *Eur. J. Pharm. Sci.* **2004**, *21*, 87–95.
[32] Wu, L.; Bai, Y. L.; Liu, M.; Li, L.; Shan, W.; Zhang, Z. R.; Huang, Y. Transport mechanisms of butyrate modified nanoparticles: Insight into "easy entry, hard transcytosis" of active targeting system in oral administration. *Mol. Pharmaceutics* **2018**, *15*, 4273–4283.
[33] Zhao, H. Y.; Chen, Y. Q.; Luo, X. Y.; Cai, M. J.; Li, J. Y.; Lin, X. Y.; Zhang, H.; Ding, H. M.; Jiang, G. L.; Hu, Y. Ligand phase separation-promoted, "squeezing-out" mode explaining the mechanism and implications of neutral nanoparticles that escaped from lysosomes. *ACS Nano* **2024**, *18*, 2162–2183.
[34] Vermeulen, L. M. P.; De Smedt, S. C.; Remaut, K.; Braeckmans, K. The proton sponge hypothesis: Fable or fact. *Eur. J. Pharm. Biopharm.* **2018**, *129*, 184–190.
[35] Fairweather, S. J.; Bröer, A.; O'Mara, M. L.; Bröer, S. Intestinal peptidases form functional complexes with the neutral amino acid transporter B^0AT1. *Biochem. J.* **2012**, *446*, 135–148.
[36] Barkin, R. J. Protein absorption: Development and present state of the subject. David Matthews, Wiley-Liss, New York, 1991, 414 pages. *JPEN J. Parenter. Enteral. Nutr.* **1992**, *16*, 186.
[37] Das, M.; Radhakrishnan, A. N. A comparative study of the distribution of soluble and particulate glycyl-l-leucine hydrolase in the small intestine. *Clin. Sci. Mol. Med.* **1974**, *46*, 501–510.
[38] Li, A. Y.; Wang, Y. P.; Li, Z. X.; Qamar, H.; Mehmood, K.; Zhang, L. H.; Liu, J. J.; Zhang, H.; Li, J. K. Probiotics isolated from yaks improves the growth performance, antioxidant activity, and cytokines related to immunity and inflammation in mice. *Microb. Cell Fact.* **2019**, *18*, 112.
[39] Li, Y. X.; Watanabe, E.; Kawashima, Y.; Plichta, D. R.; Wang, Z. J.; Ujike, M.; Ang, Q. Y.; Wu, R. R.; Furuichi, M.; Takeshita, K. et al. Identification of trypsin-degrading commensals in the large intestine. *Nature* **2022**, *609*, 582–589.
[40] Koshikawa, N.; Hasegawa, S.; Nagashima, Y.; Mitsuhashi, K.; Tsubota, Y.; Miyata, S.; Miyagi, Y.; Yasumitsu, H.; Miyazaki, K. Expression of trypsin by epithelial cells of various tissues, leukocytes, and neurons in human and mouse. *Am. J. Pathol.* **1998**, *153*, 937–944.
[41] Steinbach, E.; Masi, D.; Ribeiro, A.; Serradas, P.; Le Roy, T.; Clément, K. Upper small intestine microbiome in obesity and related metabolic disorders: A new field of investigation. *Metabolism* **2024**, *150*, 155712.
[42] Treuting, P. M.; Valasek, M. A.; Dintzis, S. M. Upper gastrointestinal tract. In *Comparative Anatomy and Histology*. Treuting, P. M.; Dintzis, S. M., Eds.; Elsevier: Amsterdam, 2012; pp 155–175.
[43] Das, P.; Majumdar, K.; Datta Gupta, S. *Surgical Pathology of the Gastrointestinal System: Volume I—Gastrointestinal Tract*, Springer: Singapore, 2022.
[44] Bennett, C. M.; Guo, M.; Dharmage, S. C. HbA_{1c} as a screening tool for detection of type 2 diabetes: A systematic review. *Diabet. Med.* **2007**, *24*, 333–343.
[45] Sherwani, S. I.; Khan, H. A.; Ekhzaimy, A.; Masood, A.; Sakharkar, M. K. Significance of HbA1c test in diagnosis and prognosis of diabetic patients. *Biomark. Insights* **2016**, *11*, 95–104.
[46] Knudsen, J. G.; Rorsman, P. β cell dysfunction in type 2 diabetes: Drained of energy. *Cell Metab.* **2019**, *29*, 1–2.
[47] Muñoz, F.; Fex, M.; Moritz, T.; Mulder, H.; Cataldo, L. R. Unique features of β-cell metabolism are lost in type 2 diabetes. *Acta Physiol.* **2024**, *240*, e14148.
[48] Wendt, A.; Eliasson, L. Pancreatic α-cells—The unsung heroes in islet function. *Semin. Cell Dev. Biol.* **2020**, *103*, 41–50.
[49] Ren, C. J.; Zhong, D. N.; Qi, Y. C.; Liu, C. Y.; Liu, X. Y.; Chen, S. H.; Yan, S.; Zhou, M. Bioinspired pH-responsive microalgal hydrogels for oral insulin delivery with both hypoglycemic and insulin sensitizing effects. *ACS Nano* **2023**, *17*, 14161–14175.
[50] Bao, X. Y.; Qian, K.; Yao, P. Oral delivery of exenatide-loaded hybrid zein nanoparticles for stable blood glucose control and β-cell repair of type 2 diabetes mice. *J. Nanobiotechnology* **2020**, *18*, 67.
[51] Müller, T. D.; Finan, B.; Bloom, S. R.; D'Alessio, D.; Drucker, D. J.; Flatt, P. R.; Fritsche, A.; Gribble, F.; Grill, H. J.; Habener, J. F. et al. Glucagon-like peptide 1 (GLP-1). *Mol. Metab.* **2019**, *30*, 72–130.
[52] Hamamoto, S.; Kanda, Y.; Shimoda, M.; Tatsumi, F.; Kohara, K.; Tawaramoto, K.; Hashiramoto, M.; Kaku, K. Vildagliptin preserves the mass and function of pancreatic β cells via the developmental regulation and suppression of oxidative and endoplasmic reticulum stress in a mouse model of diabetes. *Diabetes Obes. Metab.* **2013**, *15*, 153–163.
[53] Harrison, S. A. Liver disease in patients with diabetes mellitus. *J. Clin. Gastroenterol.* **2006**, *40*, 68–76.
[54] Barroso, E.; Jurado-Aguilar, J.; Wahli, W.; Palomer, X.; Vázquez-Carrera, M. Increased hepatic gluconeogenesis and type 2 diabetes mellitus. *Trends Endocrinol. Metab.*, in press, https://doi.org/10.1016/j.tem.2024.05.006.
[55] Xu, X. G.; Cai, Y. H.; Yu, Y. F. Effects of a novel curcumin derivative on the functions of kidney in streptozotocin-induced type 2 diabetic rats. *Inflammopharmacology* **2018**, *26*, 1257–1264.
[56] Patel, V. J.; Joharapurkar, A. A.; Shah, G. B.; Jain, M. R. Effect of GLP-1 based therapies on diabetic dyslipidemia. *Curr. Diabetes Rev.* **2014**, *10*, 238–250.